applied sciences

MDPI

Article

Material-Structure Integrated Design and Optimization of a Carbon-Fiber-Reinforced Composite Car Door

Huile Zhang [1,2,*], Zeyu Sun [1], Pengpeng Zhi [2], Wei Wang [2,3] and Zhonglai Wang [2,3,*]

[1] Shanghai Key Laboratory of Lightweight Structural Composites, Donghua University, Shanghai 201620, China; sunzeyu@dhu.edu.cn
[2] Yangtze Delta Region Institute (Huzhou), University of Electronic Science and Technology of China, Huzhou 313001, China
[3] School of Mechanical and Electrical Engineering, University of Electronic Science and Technology of China, Chengdu 611731, China
* Correspondence: zhang_tiger@foxmail.com (H.Z.); wzhonglai@uestc.edu.cn (Z.W.)

Abstract: This paper develops a material-structure integrated design and optimization method based on a multiscale approach for the lightweight design of CFRP car doors. Initially, parametric modeling of RVE is implemented, and their elastic performance parameters are predicted using the homogenization theory based on thermal stress, exploring the impact of RVE parameters on composite material performance. Subsequently, a finite element model of the CFRP car door is constructed based on the principle of equal stiffness, and a parameter transfer across microscale, mesoscale, and macroscale levels is achieved through Python programming. Finally, the particle generation and updating strategies in the Multi-Objective Particle Swarm Optimization (MOPSO) algorithm are improved, enabling the algorithm to directly solve multi-constraint and multi-objective optimization problems that include various composite material layup process constraints. Case study results demonstrate that under layup process constraints and car door stiffness requirements, plain weave, twill weave, and satin weave composite car doors achieve weight reductions of 15.85%, 14.54%, and 15.35%, respectively, compared to traditional metal doors, fulfilling the requirements for a lightweight design. This also provides guidance for the lightweight design of other vehicle body components.

Keywords: material-structure integration; fabric-reinforced composite; car door; composite layup process constraints; multiscale method

Citation: Zhang, H.; Sun, Z.; Zhi, P.; Wang, W.; Wang, Z. Material-Structure Integrated Design and Optimization of a Carbon-Fiber-Reinforced Composite Car Door. *Appl. Sci.* **2024**, *14*, 930. https://doi.org/10.3390/app14020930

Academic Editor: Joao Paulo Davim

Received: 10 December 2023
Revised: 20 January 2024
Accepted: 21 January 2024
Published: 22 January 2024

1. Introduction

The automotive industry is currently experiencing a pivotal shift to tackle essential issues in vehicle safety, energy conservation, and ecological sustainability affecting consumers and the global environment [1–3]. An effective approach to addressing the aforementioned issues involves reducing the weight of vehicles to decrease energy consumption. Research indicates that a 10% reduction in the overall vehicle equipment leads to a 6–8% decrease in energy consumption, resulting in a reduction of 1 g/km in carbon emission [1]. Therefore, substantial efforts are being made to develop vehicles that are both lightweight and crashworthy. To address the seemingly contradictory goals of lightweight design and enhanced crashworthiness, composite materials, especially carbon-fiber-reinforced plastic (CFRP), have garnered considerable attention in the scientific community [4–8]. Liu et al. [4] designed a CFRP-based electric vehicle structure, achieving a 28% reduction in weight compared to glass-fiber-reinforced plastic (GFRP) while also significantly improving the crashworthiness of the vehicle body. Under the constraints of bending stiffness, Lee et al. [9] designed, manufactured, and validated the feasibility of a CFRP roof panel. By adhering carbon fiber to the roof structure components of passenger vehicles, Bambach [10] has managed to increase the strength of the roof, effectively doubling its strength-to-weight ratio. Borazjani and Belingardi [11,12] have also conducted extensive research in a similar vein. However, the aforementioned studies primarily focus on the redesign of vehicle parts; research on complex vehicle subsystems, such as the door system, is less common.

Cheon et al. [13] designed a CFRP side-door impact beam that, compared to high-strength steel, achieves a 50% weight reduction while ensuring collision safety. Wu et al. [14] conducted a discrete optimization of the CFRP layup for the back door, achieving a more rational optimal solution compared to commercial software. Fang and Li [15] employed fiber-reinforced thermoplastic in the lightweight conceptual design of a multi-material car door, successfully achieving a 20% reduction in weight. An important feature of CFRP is the ability to shape its microstructure during the manufacturing process by selecting the type of components (i.e., reinforcement and matrix), the number and orientation of layers [16,17]. However, while the aforementioned studies have focused on the number and orientation of layers, they have not sufficiently addressed the potential for designing the microstructure.

Cheng et al. [18] implemented a microscale homogenization and macroscale optimization method, achieving a 60% weight reduction in the lightweight design of the body-in-white floor. Through a synergistic approach combining multiscale numerical simulations with experimental testing, Fang et al. [19] conducted detailed studies on the mechanical characteristics of single-ply woven composite materials. Gao et al. [20] implemented a three-scale multiscale modeling approach, which was applied to a woven composite laminate under three-point bending and to cured woven bias extension tests. Although multiscale methods have been proven effective, current studies mainly focus on simple samples, with limited multiscale design applied to door systems. Additionally, most of these designs address only car body structure replacements and seldom consider the process constraints related to CFRP layup angles. This often results in optimization outcomes that fail to meet these constraints, necessitating further refinement for practical engineering applications.

This paper proposes a material-structure integrated design and optimization approach for a CFRP car door design applied in real-world door development. The outline of the paper is as follows: Section 2 presents the analysis methods for CFRP car doors at the microscale and mesoscale and provides a detailed parameter analysis. Section 3 introduces the load conditions, constraints, and design performance criteria for CFRP car doors. Section 4 describes, in detail, the mathematical model and solution algorithm for the material-structure integrated design of CFRP car doors. Section 5 presents the derived solution outcomes, accompanied by a comprehensive analysis. Finally, Section 6 presents the main research conclusions of the paper.

2. Multiscale Modeling of Carbon-Fiber-Reinforced Composite

2.1. An Overview of Multiscale Modeling for Carbon-Fiber-Reinforced Composites

The multiscale design process of woven-fabric-reinforced composites encompasses three scales: microscale, mesoscale, and macroscale, with the structural representation of each scale illustrated in Figure 1. At the microscale, the microscale cell is composed of fiber filaments and resin, approximated from the homogenization of fiber yarns. At the mesoscale, the mesoscale cell consists of fiber yarns with a small amount of resin. Depending on the weaving pattern of the fiber yarns, mesoscale cells can be categorized into plain, twill, and satin weaves. Notably, Figure 1 shows the mesoscale cells without resin, only displaying the woven fiber yarns. At the macroscale, the laminate scale is formed by stacking multiple single-ply woven composite materials bonded together with resin. In this paper, the layup design of the car door pertains to the macroscale.

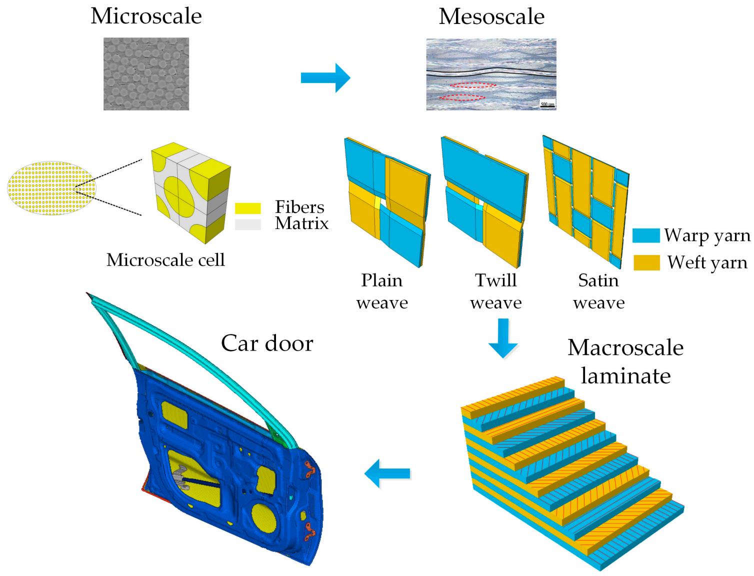

Figure 1. Flow chart of multiscale design for CFRP car door.

To predict the elastic properties of the representative volume element (RVE), this paper adopts a two-scale progressive homogenization method, which has been verified as feasible in the literature and is suitable for multiscale analysis of carbon fiber composites [18,21]. In conjunction with the finite element analysis software ABAQUS, thermal stress is applied to predict the elastic properties of the RVE. The formula for calculating the equivalent stiffness coefficients of the RVE is as follows [21,22]:

$$\boldsymbol{D}_{ijmn}^{H} = \frac{1}{|Y|}\int_{Y} \boldsymbol{D}_{ijkl}\left(\delta_{km}\delta_{ln} + \frac{\partial \psi_k^{mn}}{\partial y_l}\right)dY \tag{1}$$

where $\boldsymbol{D}_{ijmn}^{H}$ represents the equivalent stiffness matrix of the composite material, $\boldsymbol{D}_{ijkl}$ is the fourth-order stiffness matrix of the RVE, and the subscripts i, j, m, and n each represent different directions; Y denotes the region of the RVE; $\delta_{km}\delta_{ln}$ is the product of the Kronecker tensor, and ψ_k^{mn} is the displacement function.

To solve for the equivalent stiffness coefficients $\boldsymbol{D}_{ijmn}^{H}$ of the RVE in Equation (1), it is first necessary to determine the displacement function ψ_k^{mn}. The solution for the displacement function can be achieved in ABAQUS by applying thermal stress, and the functional relationship between thermal strain and temperature is as follows:

$$\varepsilon_{mn}^{c} = -k_{mn} \cdot \Delta T \tag{2}$$

where k_{mn} represents the thermal expansion coefficient, ΔT is the loading temperature, and ε_{mn}^{c} denotes the thermal strain.

Through theoretical derivation, the displacement function in Equation (1) can be converted into the form of thermal expansion coefficient, as follows:

$$\boldsymbol{D}_{ijmn}^{H} = \frac{1}{|Y|}\int_{Y} \boldsymbol{D}_{ijkl}\left[\frac{1}{2}\left(\frac{\partial \psi_k^{mn}}{\partial y_l} + \frac{\partial \psi_l^{mn}}{\partial y_k}\right) + k_{mn} \cdot \Delta T\right]dY \tag{3}$$

In ABAQUS, Multi-Point Constraints (MPC) are applied, and the binding constraint is used to implement periodic boundary conditions. A Fortran subroutine is written to apply thermal stress, and a Python script is developed to read stress-strain information, ultimately solving for the homogenization coefficients of the RVE. Due to space limitations, the two-scale progressive homogenization method is not described in detail; interested readers may refer to the literature for more information [17,18,21].

2.2. Microscale Model Simulation Analysis

To achieve the material-structure integrated design of CFRP car doors, understanding the microscale properties of carbon fiber composites is essential. Therefore, this section conducts a detailed study of the microscale dimensions of carbon fiber composites, encompassing the establishment of microscale cells, multiscale analysis of these cells, and the impact of microscale parameters on the elastic properties of the composites.

2.2.1. Microscale Model Simulation Analysis Method

The woven yarns in CFRP are composed of fiber filaments and resin, as shown in Figure 2. The cross-sectional structure of the woven yarns is observed using an electron microscope (model JSM-IT300LA) to obtain a realistic microscale model, which is then approximated to an equivalent microscale cell through homogenization. As can be seen from Figure 2, the microscale cell is composed of carbon fiber filaments, represented by the yellow area, and resin, represented by the gray area. The geometric parameters of the microscale cell mainly include the diameter of the fiber filaments, the thickness of the cell, and the half-side length (x_1) of the cell. Previous literature studies have shown that the main factor affecting the elastic properties of the microscale cell structure is the fiber volume fraction (V_f) [21,23]. Therefore, in this paper, while the fiber diameter and cell thickness are fixed, different V_f are obtained by setting different half-side lengths x_1 for the microscale cell, that is, choosing the x_1 of the microscale cell shown in Figure 2 as the microscale design variable.

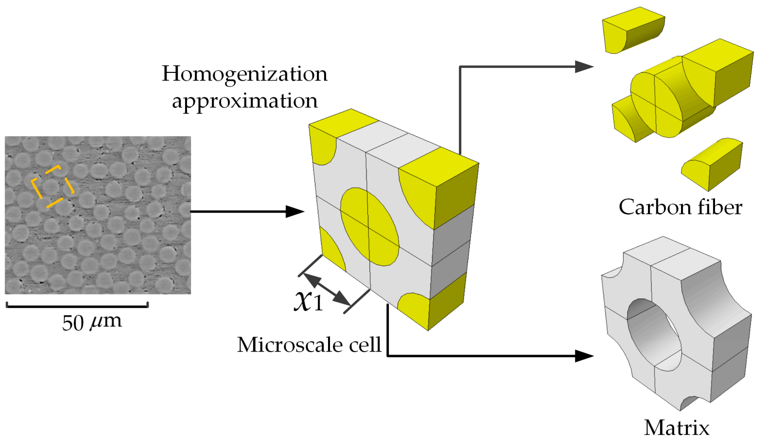

Figure 2. Schematic view of microscale cell.

In this study, T700-12k carbon fibers are used, and the resin selected is EPOLAM 5015 RESIN epoxy. The mechanical properties of both the fibers and the resin are presented in Table 1.

Table 1. Material properties of T700/EPOLAM 5015 RESIN used in the multiscale design.

Material	E_1/GPa	E_2 = E_3/GPa	G_{12} = G_{13}/GPa	G_{23}/GPa	$\mu_{12} = \mu_{13}$	μ_{23}
Fiber	227.0	13.4	6.8	4.8	0.2	0.25
Matrix	3.3	-	-	-	0.35	-

A microscale cell model, as depicted in Figure 2, was developed in ABAQUS for the predictive analysis. In this model, the fiber-reinforced phase is represented by the yellow region, while the resin matrix is indicated by the gray area, comprising a fiber volume fraction of 51%. The analysis involved constructing a finite element model of the microscale cell in ABAQUS, inputting material parameters for each component as listed in Table 1, specifying material orientations, and setting up a thermal stress analysis step. The mesh was created using C3D8R elements with a side length of 0.4 mm. A custom Fortran subroutine was developed to define specific variables, and binding contact techniques were applied to enforce periodic boundary conditions on the microscale cell. Computations were executed in ABAQUS, with Figure 3 illustrating the resultant equivalent stress distribution in the microscale cell under six distinct thermal stress scenarios. Figure 3a,b displays the tensile scenarios. Specifically, Figure 3a shows stretching along the fiber direction, with the fiber serving as the main load-bearing component. The stress levels in Figure 3b,c are nearly identical, with the primary distinction being a 90° rotation in the stress distribution around axis one, further validating the reliability of the thermal stress-based analysis method. Figure 3d–f illustrate shear conditions, whereas Figure 3d,e exhibits almost the same stress values, yet the stress distribution is rotated 90° around axis one. Post-calculation, a Python script was employed to extract the results, facilitating the determination of equivalent elastic properties for the microscale cell.

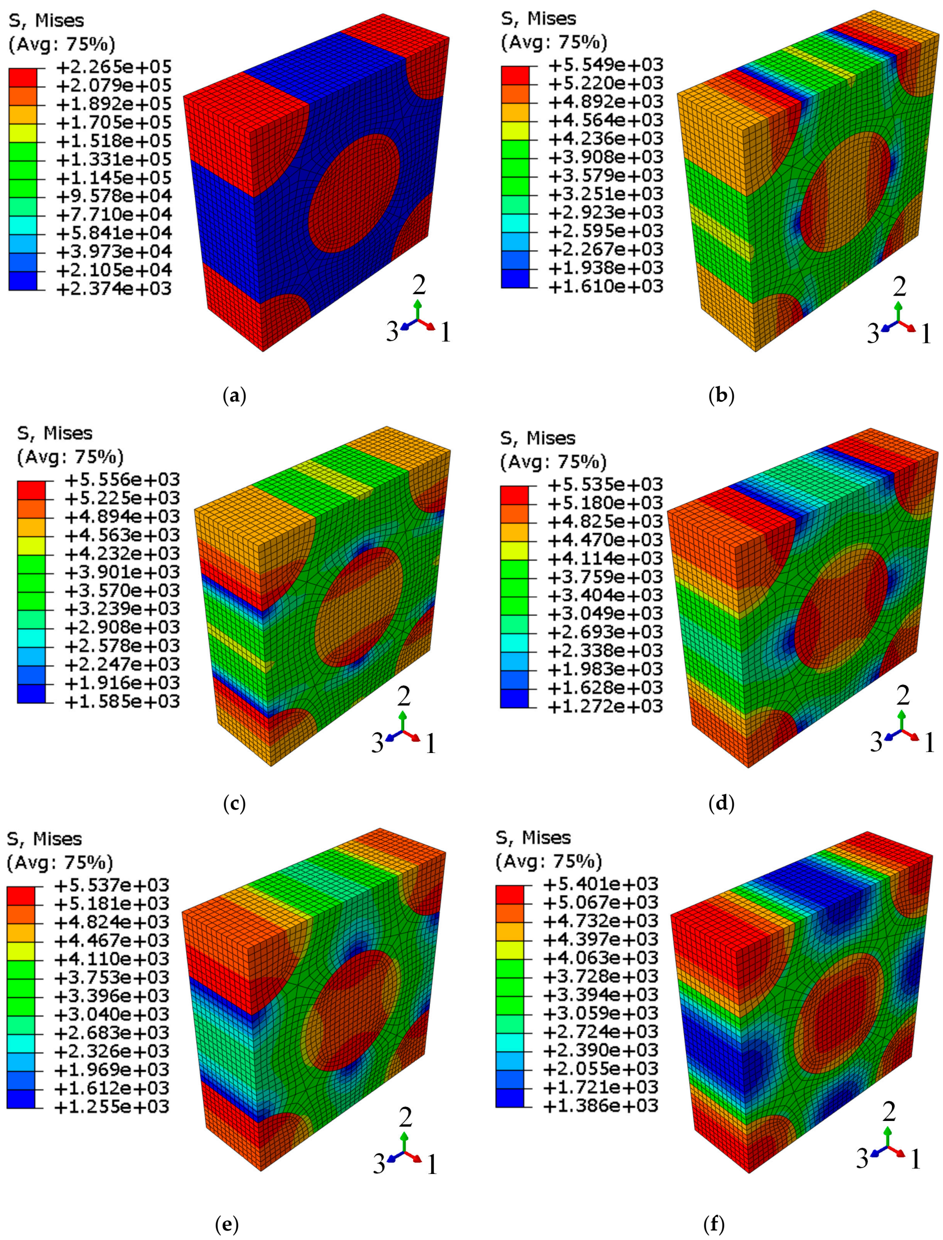

Figure 3. Equivalent stress contour result of different thermal stress conditions: (**a**) S^{11}; (**b**) S^{22}; (**c**) S^{33}; (**d**) S^{12}; (**e**) S^{13}; (**f**) S^{23}.

To verify the effectiveness of the homogenization theory based on thermal stress for predicting the elastic properties of the microscale cell, the computational results of this paper are compared with experimental values from the literature [20], as shown in Table 2. The table reveals that the maximum discrepancy occurs in the Poisson's ratio, with a difference of 3.03%. Considering the inherent uncertainties in experimental procedures, it can be concluded that this method effectively predicts the elastic parameters of composite materials.

Table 2. Comparison of simulation results and experimental results.

Material Properties	E_1/GPa	$E_2 = E_3$/GPa	$G_{12} = G_{13}$/GPa	G_{23}/GPa	$\mu_{12} = \mu_{13}$	μ_{23}
Simulation result	115.12	6.04	3.44	4.8	0.34	0.25
Experimental result	113.57	6.10	3.46	-	0.33	-
Error	1.6%	0.98%	0.59%	-	3.03%	-

2.2.2. Influence of Microscale Parameters on Elastic Properties

The woven yarns in CFRP are composed of fibers and resin, and the proportion of each component greatly influences the elastic properties of the composite. To investigate the impact of the V_f in the microscale cell on the elastic parameters of the composite material, this study conducts an analysis of microscale cells with different V_f using the homogenization method based on thermal stress described in Section 2.2.1. The results are presented in Figure 4.

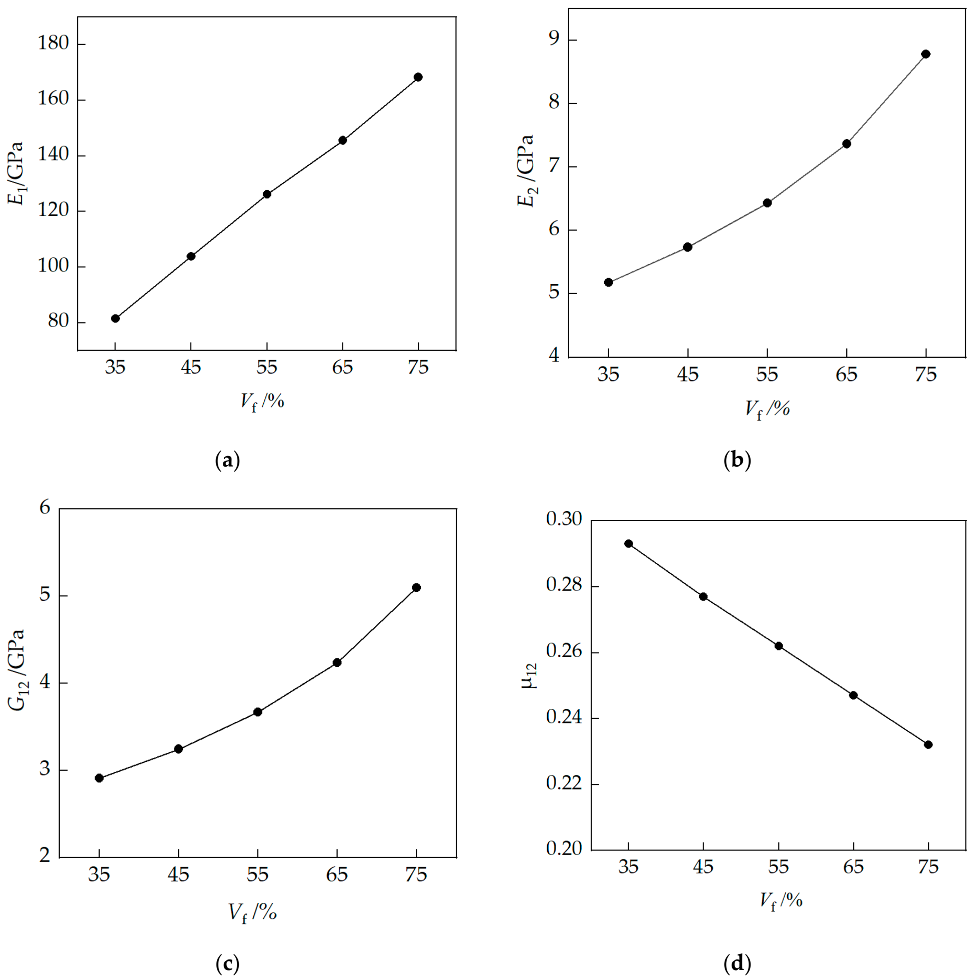

Figure 4. The influence of fiber volume fraction on the elastic properties of CFRP: (**a**) E_1; (**b**) E_2; (**c**) G_{12}; (**d**) μ_{12}.

As illustrated in Figure 4, the V_f significantly influences the elastic behavior of composite materials. Generally, an increase in V_f leads to a marked rise in the elastic modulus and a concurrent reduction in Poisson's ratio, indicating an enhancement in overall mechanical performance with higher fiber content. Notably, the elastic modulus E_1 exhibits a near-linear increment with V_f, likely due to the axial properties of fibers being the predominant factor, considering the modulus of the resin is much lower than that of the fibers. On the other hand, both E_2 and G_{12} show an accelerated increase with higher V_f. This trend can be explained by the initial dominance of resin properties when the fiber content is low, resulting in lower values for E_2 and G_{12}. As the fiber content increases, the influence of fibers becomes more pronounced, leading to the observed enhanced growth rates of E_2 and G_{12} with increasing V_f.

2.3. Mesoscale Model Simulation Analysis

To achieve the material-structure integrated design and optimization for CFRP car doors, it is necessary not only to understand the characteristics of microscale cells but also to explore the effects of mesoscale cell parameters on the elastic properties of single-ply woven composite materials. In light of this, this section focuses on the construction and multiscale analysis of mesoscale cells and examines the impact of mesoscale cell parameters on the elastic behavior of single-ply woven composites, featuring an extensive examination of prevalent woven mesoscale cells.

2.3.1. Mesoscale Model Simulation Analysis Method

Two-dimensional woven composite materials are created by intertwining fiber yarns using various weaving techniques and combining them with a small amount of resin, resulting in a distinct type of composite material. Depending on the weaving technique of the fiber yarns, these composites can be classified into plain weave, twill weave, and satin weave, as depicted in Figures 5 and 6. The current section delves into the mesoscale cell construction, specifically focusing on plain weave composites. Electron microscope scans of plain weave composite cross-sections show that fiber yarns form a carbon fiber fabric with a wavy pattern through weaving. For the multiscale analysis of mesoscale cells, the mesoscale structure of plain weave composites needs simplification. The division of mesoscale cells for plain weave composites is illustrated in Figure 7.

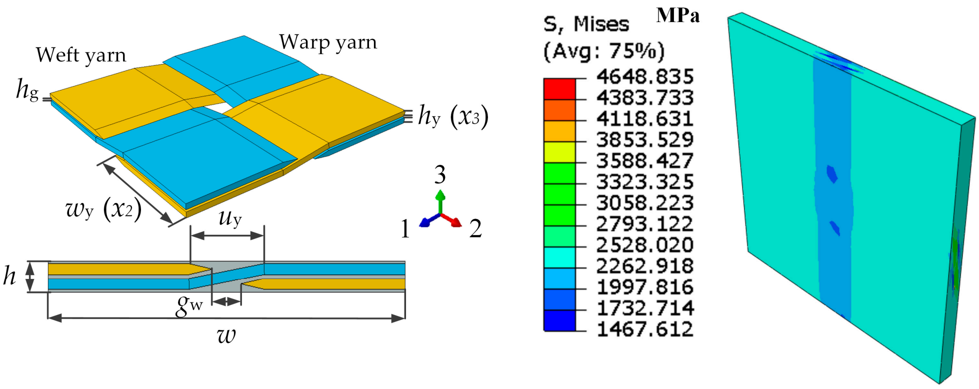

(**a**) (**b**)

Figure 5. The plain weave mesoscale cell structure: (**a**) Plain weave mesoscale cell structure parameters; (**b**) Equivalent stress contour result of plain weave mesoscale cell structure.

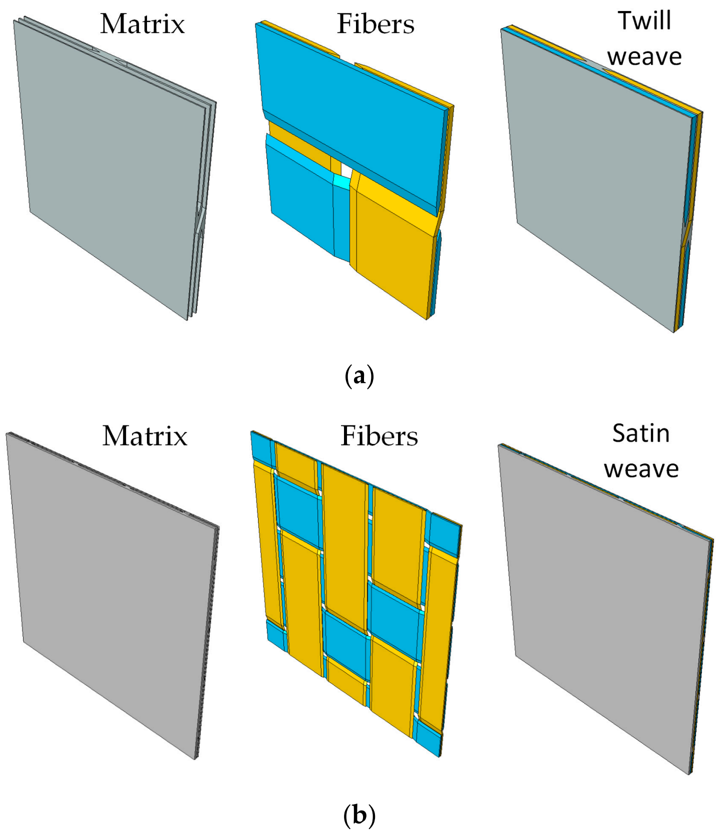

Figure 6. Mesoscale cell structure: (**a**) The twill weave mesoscale cell structure; (**b**) The satin weave mesoscale cell structure.

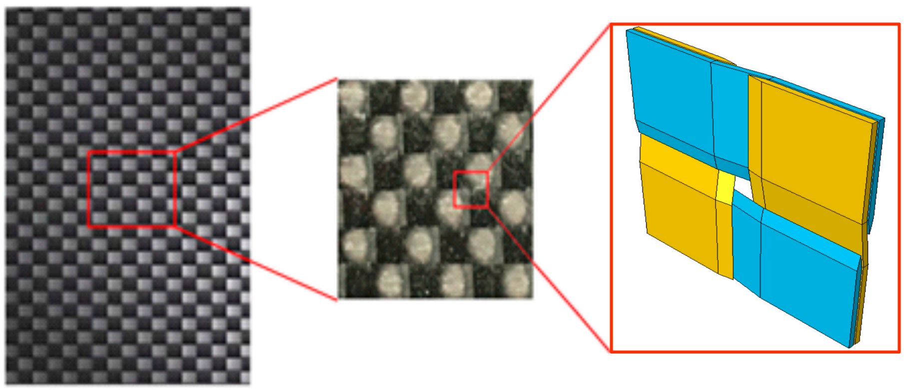

Figure 7. Schematic view of plain weave mesoscale cell structure.

In developing mesoscale cell models for plain weave composites, Ishikawa and Chou [24] initially introduced the concept of mesoscale cells in fabrics, representing the yarns as zigzag lines. Pochiraju et al. [25] enhanced this model by substituting the zigzag transitions with sine curve transitions, thereby bringing the model closer to actual structures. Further model simplification was proposed by Whitney et al. [26], who suggested linear transitions for yarn curves. This approach not only simplified the modeling process but also ensured that the resulting model met design requirements. Consequently, this study adopts the approach proposed by Whitney to establish the mesoscale structure of plain weave composite materials, as illustrated in Figure 5a.

From Figure 5a, it is evident that the mesoscale cell primarily comprises warp yarns, weft yarns, and resin. The geometric parameters of the mesoscale cell are defined as follows: h_g is the thickness of resin between adjacent fiber yarns, h_y denotes the thickness of fiber yarns, w_y represents the width of the yarns, u_y is the distance between adjacent yarns, h indicates the total thickness of the mesoscale cell, g_w refers to the width of the curved part of the yarns, and w is the overall width of the mesoscale cell. Literature studies have shown that the volume fraction of fiber yarns (V_y) is a crucial factor influencing the elastic properties of the mesoscale cell [17,23]. Therefore, in this study, all parameters except w_y and h_y are kept constant, and the fiber yarn volume fraction is controlled by adjusting the widths w_y and thicknesses h_y of the yarns. That is, w_y and h_y, shown in Figure 5a, are selected as the design variables for the mesoscale, denoted as x_2 and x_3, respectively.

In woven composite materials, mesoscale fiber yarns are comprised of numerous filaments and resin. To predict the properties of woven fiber composites using the thermal stress method, it is necessary to input the material parameters of both fiber yarns and resin. In this section, unidirectional fiber yarns with a fiber volume fraction of 51% and EPOLAM 5015 RESIN epoxy are used as mesoscale material inputs, as discussed in Section 2.2, with specific parameters detailed in Table 3. A mesoscale cell model, as depicted in Figure 6a, is established in ABAQUS, and the homogenization method based on thermal stress, introduced in Section 2.1, is applied for analysis. Figure 5b shows the equivalent stress contour map obtained from the finite element analysis.

Table 3. Material properties of mesoscale cell.

Material	E_1/GPa	$E_2 = E_3$/GPa	$G_{12} = G_{13}$/GPa	G_{23}/GPa	$\mu_{12} = \mu_{13}$	μ_{23}
Cabon yarn	115.12	6.04	3.44	4.8	0.34	0.25
Matrix	3.3	-	-	-	0.35	-

Applying the same analysis method as described earlier, the twill and satin weave composites depicted in Figure 6 are also analyzed, and the elastic parameters of their mesoscale cells are calculated and included in Table 4. The data in the table indicate that the elastic properties of mesoscale cells with different weaving patterns do not vary significantly.

Table 4. Elastic properties of mesoscale cell.

Material	$E_1 = E_2$/GPa	E_3/GPa	$G_{13} = G_{23}$/GPa	G_{12}/GPa	$\mu_{13} = \mu_{23}$	μ_{12}
Plain weave	24.09	5.62	1.64	1.73	0.47	0.06
Twill weave	28.65	5.83	1.81	1.69	0.46	0.05
Satin weave	21.05	5.66	1.68	1.82	0.45	0.06

2.3.2. Influence of Mesoscale Parameters on Elastic Properties

Carbon fiber woven composites are composed of fiber yarns and resin, as shown in Figure 6. The performance of each component greatly influences the overall properties of the composite material. To study the impact of fiber yarn volume fraction (V_y) in the mesoscale cells on the elastic parameters of the composite material, this section conducts an analysis of mesoscale cells with different fiber yarn volume fractions based on the prediction method described in Section 2.3.1. The results are presented in Figure 8.

Figure 8 indicates that the V_y significantly influences the elastic properties of single-ply woven composites. Generally, an increase in V_y leads to an increase in elastic modulus and a decrease in Poisson's ratio for these composites, suggesting that their overall mechanical performance improves with higher fiber yarn content. Unlike the influence of fiber volume fraction on microscale cell elastic properties, an increase in fiber yarn volume fraction in single-ply woven composites results in an approximately linear increase in elastic modulus. This trend is likely due to the elastic modulus of fiber yarns in mesoscale cells being substantially higher than that of the resin; thus, the properties of the fiber yarns predominantly determine the predicted elastic performance.

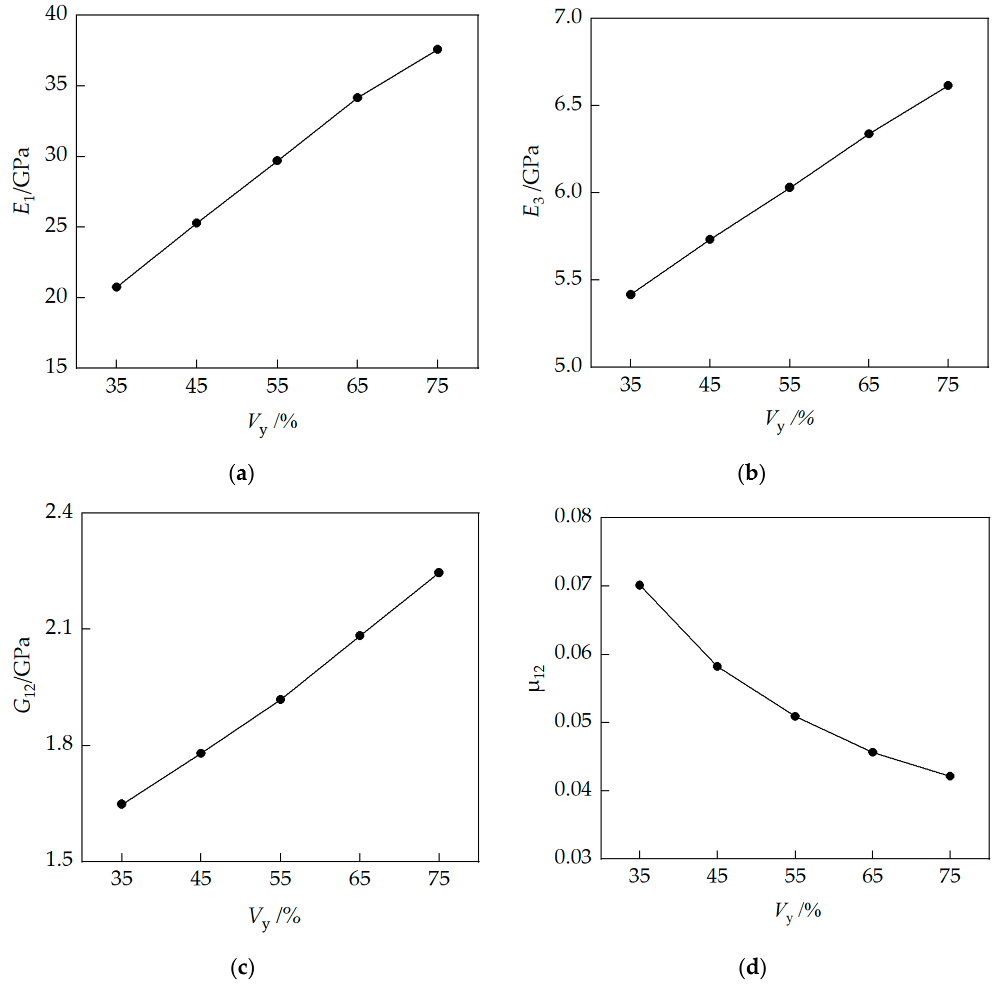

Figure 8. The influence of yarn volume fraction on the elastic properties of CFRP: (**a**) E_1; (**b**) E_3; (**c**) G_{12}; (**d**) μ_{12}.

3. Carbon-Fiber-Reinforced Composite Car Door

3.1. The Initial Car Door Model

This paper selects a car door under development by a certain automotive manufacturer as the research subject. The car door system mainly comprises the window frame, lock core reinforcement plate, glass frame reinforcement, outer panel, inner panel, impact beam mounting plate, impact beam, hinge mounting plate, door hinge, etc., with each component illustrated in Figure 9. In the initial design, the total weight of the car door is 15.96 kg, with the inner panel weighing 6.12 kg, accounting for 38.34% of the total mass. This highlights the crucial role of lightweight design for the inner panel in the overall weight reduction of the car door system.

In the lightweight design of car doors, to ensure sufficient comfort and safety during vehicle operation and usage, the doors must possess adequate stiffness [14,27]. The indicators for measuring door stiffness include upper torsional stiffness, lower torsional stiffness, and sagging stiffness, all of which must meet the design requirements of the manufacturer. In modal analysis, a free modal analysis approach is employed for the car door, with the requirement that the first natural frequency exceeds 35 Hz to prevent resonance. Based entirely on the SAIC Passenger Car Door Rigidity Test Specification, the loading conditions and constraints for the door's stiffness are depicted in Figure 10. The specific constraints and design criteria are detailed in Table 5.

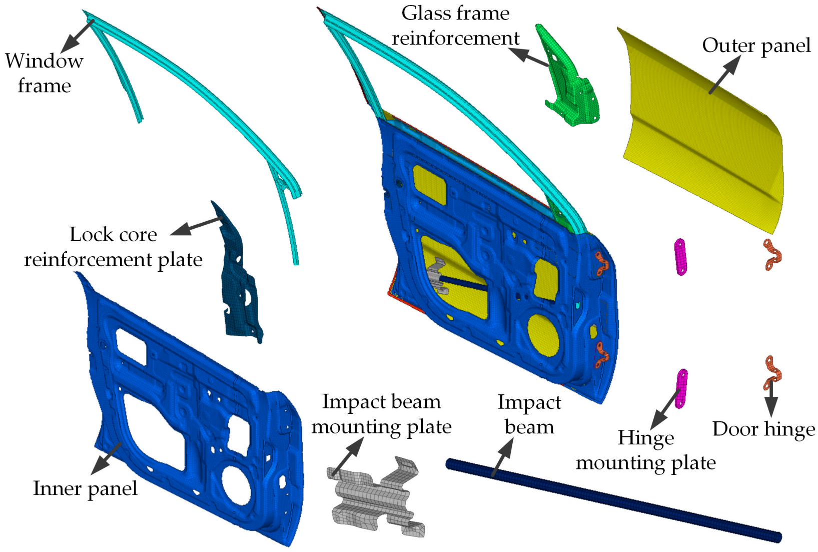

Figure 9. Exploded view of the door assembly.

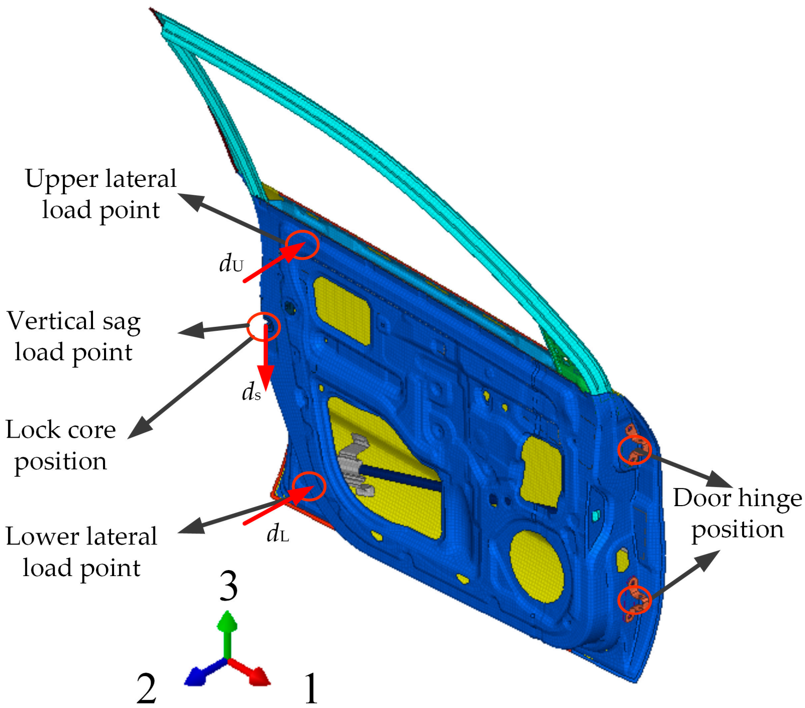

Figure 10. Loading and boundary conditions for car door stiffness.

In the sagging condition, the hinges are constrained in all six degrees of freedom, while the lock core is constrained in the first and second directions, with a 900 N force applied in the third direction at the lock core position. The vertical displacement d_s at the lock core position must be less than 4.5 mm. For upper torsional stiffness, the hinges are constrained in all six degrees of freedom, while the lock core is constrained in the first, second, and third directions, with a −900 N load applied in the second direction at a displacement of 50 mm below the window edge, and the upper-end displacement d_U of the door must be less than 10 mm. In lower torsional stiffness, the hinges are constrained in all six degrees of freedom, while the lock core is constrained in the first, second, and third directions, with a −900 N load applied in the second direction at a distance of 50 mm above the door sideline, and the lower end displacement d_L of the door must be less than 7 mm.

Table 5. Load and constrained conditions of different stiffness cases.

Stiffness Cases	Constrained Conditions	Load Conditions	Performance Indicators
Vertical sag	Constrain the six degrees of freedom at the hinge, and constrain the degrees of freedom in directions 1 and 2 of the lock core.	Apply a force of 900 N in 3 directions at the lock core.	Displacement in 3 directions at the loading point, d_s < 4.5 mm
Upper torsional stiffness	Constrain the six degrees of freedom at the hinge, and constrain the degrees of freedom in directions 1, 2, and 3 of the lock core.	Apply a force of −900 N in 2 directions at a distance of 50 mm below the window edge.	Maximum displacement in 2 directions at the upper part of the car door, d_U < 10 mm.
Lower torsional stiffness	Constrain the six degrees of freedom at the hinge, and constrain the degrees of freedom in directions 1, 2, and 3 of the lock core.	Apply a force of −900 N in 2 directions at a distance of 50 mm above the door edge.	Maximum displacement in 2 directions at the Lower part of the car door, d_L < 7 mm.

3.2. Carbon-Fiber-Reinforced Composite Car Door

In the material-structure integrated design and optimization of CFRP car doors, to ensure that the composite car door achieves a stiffness comparable to that of the original metal door, this paper adopts the principle of equal stiffness for the replacement design of the car door inner panel. The specific implementation method involves achieving similar stiffness properties between the CFRP door and the metal door through preliminary design, which includes adjusting the microscale cell fiber volume fraction V_f, mesoscale cell thickness h, and the number of layup layers N. The specific stiffness criteria constraints are as follows:

$$\begin{cases} d_s(\boldsymbol{T}) < 4.5\ \text{mm} \\ d_U(\boldsymbol{T}) < 10\ \text{mm} \\ d_L(\boldsymbol{T}) < 7\ \text{mm} \\ \boldsymbol{T} = [V_f, h, N]^{\mathrm{T}} \end{cases} \tag{4}$$

where $\boldsymbol{T}$ represents the vector of design variables, d_s is the sagging displacement, d_U is the upper torsional displacement, and d_L is the lower torsional displacement.

The preliminary selection range for the V_f is between 20% and 70%, the thickness range for mesoscale cell h is between 0.2 mm and 0.4 mm, and the number of layup layers N is between 8 and 16. Sample points are selected within the design space for simulation calculations. The final results show that when the V_f is 35%, the thickness of the mesoscale cell h is 0.35 mm, and the number of layup layers N is 12, the stiffness of the CFRP car door meets the constraints of Equation (4). The performance comparison of the initial composite car door design with the original metal door is shown in Table 6. The table reveals that the CFRP door not only meets the stiffness constraints but also closely matches the stiffness performance of the initial metal door. Therefore, the initial design of the CFRP car door is determined with a microscale fiber V_f of 35%, and the single-layup thickness h and the number of layup layers N are set at 0.35 mm and 12, respectively.

Table 6. Initial performance indicators of CFRP car door.

Performance Indicators	Threshold	Initial Car Door	CFRP Car Door
Mass (kg)	-	15.96	13.47
First-order natural frequency (Hz)	>35	38	42
Vertical sag d_s (mm)	<4.5	3.66	3.45
Upper lateral d_U (mm)	<10	9.85	7.56
Lower lateral d_L (mm)	<7	6.63	5.48

4. Methodology for Design and Optimization of Material-Structure Integration

4.1. Definition of the Optimization Model

In the car door design process, multiple, often conflicting, objectives arise [27]. For instance, increasing the fiber volume fraction enhances door stiffness but may compromise its weight reduction. To balance various performance indicators of the car door, this paper selects the mass M of the CFRP car door and the sagging displacement d_{s} as the objectives, with the upper torsional displacement d_{U}, lower torsional displacement d_{L}, first natural frequency f, Tsai-Wu failure criterion $TWSI$ [28], and layup process as constraints. The optimization mathematical model is constructed as follows:

$$\begin{cases} \text{Find}: & \boldsymbol{X} \\ \text{Minimize}: & M(\boldsymbol{X}),\ d_s(\boldsymbol{X}) \\ \textit{Subject to}: & d_U(\boldsymbol{X}) < 10\ \text{mm} \\ & d_L(\boldsymbol{X}) < 7\ \text{mm} \\ & f(\boldsymbol{X}) > 35\ \text{Hz} \\ & 0 \le TWSI \le 1 \\ & \boldsymbol{X} = [x_1, x_2, x_3, x_4 \cdots x_{15}]^{\mathrm{T}} \end{cases} \tag{5}$$

where design variables x_1–x_3 are continuous variables, variable x_1 represents the half-side length of the microscale cell (as shown in Figure 2), variable x_2 represents the width of the fiber yarn (as shown in Figure 5), and variable x_3 represents the thickness of the fiber yarn (also shown in Figure 5). Design variables x_4–x_{15} are discrete variables, with each design variable offering a choice among four layup angles: $-45°$, $0°$, $45°$, and $90°$.

To ensure that the optimization results comply with the layup process constraints for composite materials, this paper proposes the following implementation methods for common process constraints:

- Layup orientation principle, selecting $0°$, $90°$, and $\pm 45°$ as the layup angles;

Discrete integer variables 0, 1, 2, and 3 are used to represent layup angles of $-45°$, $0°$, $45°$, and $90°$, respectively, with N_u denoting the angle of the uth layup. During the initialization and particle updating stages of the Multiple Objective Particle Swarm Optimization (MOPSO) algorithm [29,30], the layup orientation constraint is enforced by modifying the methods for generating and updating particles.

- Balanced symmetry layup principle;

The balanced symmetry layup requires that the laminate is designed with a symmetrical structure during layup design, effectively preventing warping of the laminate under load. This constraint can be represented by Equation (6):

$$N_u - N_{13-u} = 0 \; u = 1, 2, \cdots 6 \tag{6}$$

In Equation (6), when the layup angle of the uth layer is between $0-3$, the layup angle of the (13-u)th layer is also between $0-3$ and appears paired with it.

- $\pm 45°$ single-ply symmetrical layup principle

To prevent warping deformation of the laminate under load, when there are $\pm 45°$ layups in the laminate, there must be $\mp 45°$ layups appearing in pairs with them. The implementation of this constraint is shown in Equation (7):

$$\begin{array}{lll} N_{13-u} = 0 & N_u = 2 & u = 1, 2, \cdots 6 \\ N_{13-u} = 2 & N_u = 0 & u = 1, 2, \cdots 6 \end{array} \tag{7}$$

In Equation (7), when the layup angle of the uth layer is 2 ($45°$), the layup angle of the (13-u)th layer is 0 ($-45°$); similarly, when the layup angle of the uth layer is 0 ($-45°$), the layup angle of the (13-u)th layer is 2 ($45°$).

- Avoiding the consecutive layup of four layers with the same angle.

When a composite laminate has too many identical and consecutive layups, there is an increased risk of delamination. To prevent this, generally, no more than four layers of the same layup are allowed in the design of composite materials. This manufacturing constraint is managed by evaluating the design variables generated during the optimization process to avoid such occurrences.

4.2. Optimization Design Methodology

The development of advanced computational methods, such as optimization techniques and finite element analysis, has significantly improved the efficiency of engineering design [31,32]. Building upon this progress, this paper extends the multiscale material-structure integrated analysis method for carbon-fiber-reinforced plastics (CFRP), introduced in Section 2, to propose an integrated design method specifically for CFRP car doors, as illustrated in Figure 11. The approach involves

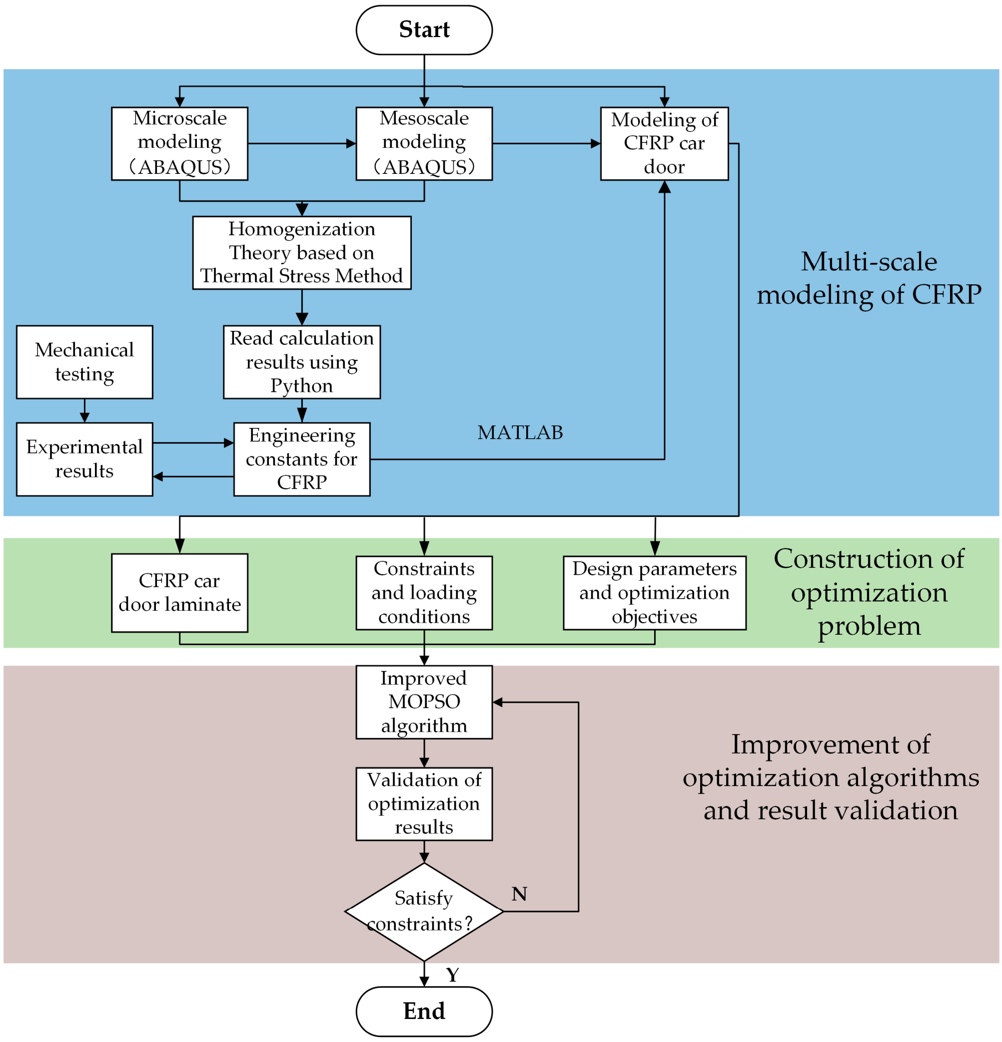

Figure 11. Flow chart of the design and optimization of material-structure integration.

Step 1: CFRP multiscale modeling and elastic parameters prediction.

Python programming is used for parametric modeling of microscale and mesoscale cells, and the homogenization theory based on thermal stress is employed to predict the elastic properties of the cells.

Step 2: Construction and parameter transfer of the CFRP car door model.

Based on the principle of equal stiffness, a CFRP car door model is established, and programming is utilized to transfer parameters from microscale to mesoscale and then to the car door material, thereby constructing the optimization model for the CFRP car door.

Step 3: Proposal of an integrated optimization design algorithm for CFRP car doors.

The initialization and updating strategies of particles in the particle swarm algorithm are improved, enabling the improved algorithm to solve multiscale optimization problems, including layup process constraints.

5. Results and Discussion

By applying the material-structure integrated optimization algorithm presented in Section 4, we successfully addressed the multiscale optimization design challenges for plain weave, twill, and satin weave composite car doors, considering both scenarios with and without process constraints. The converging Pareto solution sets are shown in Figures 12–14 [33]. Overall, it is observed that the sagging stiffness and the mass of the CFRP car doors are two conflicting performance indicators. This means that if a solution with a lower door mass is selected from the solution set, it will inevitably have a larger sagging displacement, i.e., lower sagging stiffness, and vice versa. Furthermore, the solution sets considering process constraints and those not considering them show similar patterns of variation, but their distribution positions are significantly different. Specifically, the solution sets considering process constraints are mostly located in the upper right area of those not considering constraints, with this trend being most evident in the twill composite car door, as shown in Figure 13. The possible reason for this phenomenon is that when process constraints are considered, the feasible domain of design variables decreases. Some designs with lower mass and higher stiffness may not meet the layup process constraints of carbon fiber composites. Therefore, in the Pareto solution set, considering process constraints shifts the set towards the upper right, losing some performance indicators. To clarify this point further, the solution set within the circle in Figure 14 is examined: it was found that the solution set not considering process constraints includes layup designs with four consecutive layers at 0°, whereas the set considering process constraints, although slightly compromising on door mass and sagging stiffness, fully meets the requirements proposed in Section 4.1. In summary, although the performance parameters of the multiscale design of CFRP considering process constraints are slightly deteriorated, the solution set meets layup process requirements, avoiding design flaws due to poor layup design.

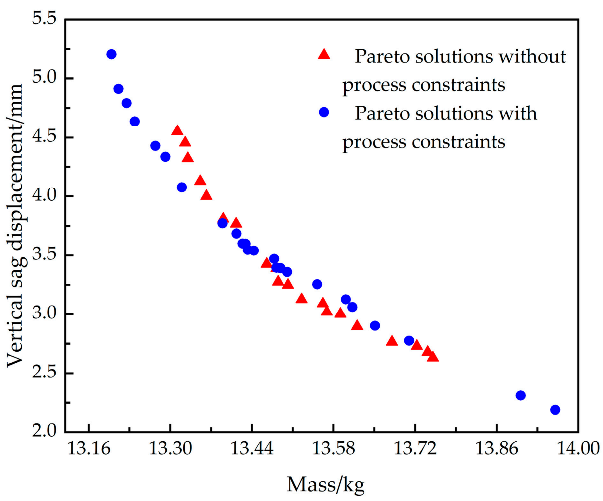

Figure 12. Pareto solutions for integrated design of plain weave.

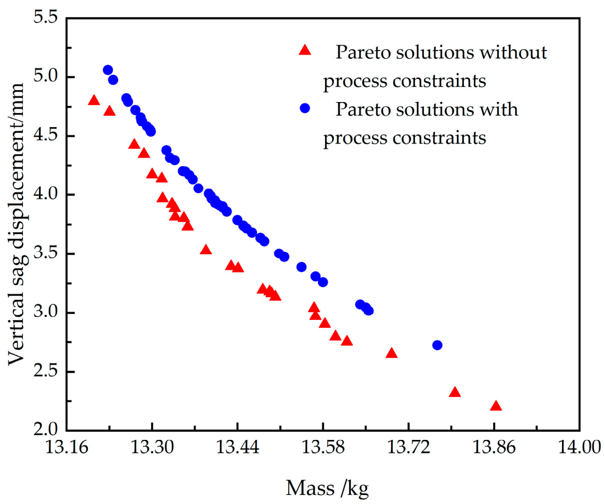

Figure 13. Pareto solutions for integrated design of twill weave.

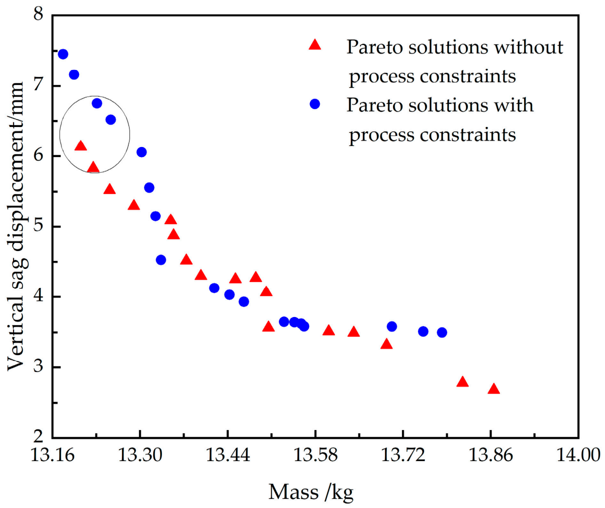

Figure 14. Pareto solutions for integrated design of satin weave.

Although the Pareto solution set offers many feasible alternatives, selecting an appropriate solution for guiding engineering design is crucial in practical applications. To reasonably balance the conflicting performance indicators of door mass and sagging stiffness, this paper employs the minimum distance selection method [34], choosing the best solutions from the sets in Figures 12–14. The optimal solution for the plain weave car door: microscale cell fiber volume fraction of 59.49%, mesoscale cell fiber yarn volume fraction of 49.11%, laminate layup angles of [0°, 45°, −45°, 0°, 90°, 0°, 0°, 90°, 0°, 45°, −45°, 0°]. The optimal solution for the twill weave car door: microscale cell fiber volume fraction of 62.25%, mesoscale cell fiber yarn volume fraction of 49.35%, laminate layup angles of [90°, 45°, 90°, 0°, 0°, 90°, 90°, 0°, 0°, 90°, −45°, 90°]. The optimal solution for the satin weave car door: microscale cell fiber volume fraction of 39.37%, mesoscale cell fiber yarn volume fraction of 70.23%, laminate layup angles of [0°, 45°, 0°, 90°, 0°, 90°, 90°, 0°, 90°, 0°, −45°, 0°]. The chosen optimal solutions all meet the process requirements in terms of layup angles.

To further illustrate the advantages of CFRP car doors, performance indicators such as mass, sagging stiffness, and upper torsional stiffness for plain, twill, and satin weave composite car doors are extracted and listed in Table 7. The data from the table show that, on the one hand, the optimized plain, twill, and satin weave car doors meet performance requirements in terms of sagging stiffness, upper torsional stiffness, lower torsional stiffness, and first natural frequency. On the other hand, compared to traditional metal car doors, the mass of the optimized plain, twill, and satin weave solutions is reduced by 15.85%, 14.54%, and 15.35%, respectively. Overall, compared to the original metal doors, the car doors made of CFRP demonstrate significant weight reduction effects, with plain weave composite car doors achieving the best weight reduction of 15.85%. While achieving a lightweight design, the stiffness of the composite car doors is also substantially enhanced.

Table 7. Comparison of performance indicators between CFRP and metal car doors.

Performance Indicators	Threshold	Initial Metal	Plain Weave	Twill Weave	Satin Weave
First-order natural frequency (Hz)	>35	36.6	37	38	36
Vertical sag d_s (mm)	<4.5	9.85	3.55	3.72	4.4
Upper lateral d_U (mm)	<10	6.63	7.55	7.15	8.83
Lower lateral d_L (mm)	<7	38	5.48	5.31	6.79
Mass M (kg)	-	15.96	13.43	13.48	13.51
Lightweight level (%)	-	-	15.85	14.54	15.35

6. Conclusions

In this study, a comprehensive, integrated design methodology for multiscale materials and structures was developed specifically for woven-reinforced composites, demonstrated through a case study on a car door system. The main conclusions are as follows:

(1) A predictive model for the microscale and mesoscale elastic properties of woven-reinforced composites was established. It was observed that as the fiber volume fraction V_f in the microscale cells increases, E_1 linearly increases, whereas E_2 and G_{12} increase nonlinearly with an escalating growth rate. Furthermore, increasing the fiber yarn volume fraction V_y in mesoscale cells leads to a linear rise in parameters like E_1, E_3, and G_{12}.

(2) The particle generation strategy in the MOPSO algorithm was refined to apply the layup process constraints for composite materials. The optimization showed that the enhanced algorithm effectively generates Pareto solution sets meeting process constraints, thereby boosting the multiscale optimization method's applicability in engineering.

(3) Applying the proposed integrated optimization approach to the design of plain, twill, and satin weave composite car doors resulted in significant achievements. Post-optimization, the CFRP car doors showed a weight reduction of 15.85%, 14.54%, and 15.35% compared to traditional metal doors, meeting all performance and layup process constraints. These results underscore the efficacy of the developed universal design method in facilitating lightweight automotive design.

Author Contributions: Conceptualization, H.Z. and Z.S.; methodology, H.Z.; software, H.Z.; validation, H.Z., Z.S. and P.Z.; formal analysis, P.Z.; investigation, H.Z.; resources, W.W.; data curation, H.Z.; writing—original draft preparation, H.Z.; writing—review and editing, H.Z.; visualization, Z.W.; supervision, Z.W.; project administration, H.Z.; funding acquisition, Z.S. All authors have read and agreed to the published version of the manuscript.

Funding: This research work was supported by the Open Fund Project of the Shanghai Key Laboratory of Lightweight Structural Composites (Grant No. 2232021A4-06) and the S&T Special Program of Huzhou (Grant No. 2023GZ09).

Institutional Review Board Statement: Not applicable.

Informed Consent Statement: Not applicable.

Data Availability Statement: The original contributions presented in the study are included in the article, further inquiries can be directed to the corresponding authors.

Conflicts of Interest: The authors declare no conflicts of interest.

References

1. Wazeer, A.; Das, A.; Abeykoon, C.; Sinha, A.; Karmakar, A. Composites for electric vehicles and automotive sector: A review. *Green Energy Intell. Transp.* **2023**, *2*, 100043. [CrossRef]
2. Ren, Y.; Liu, Z.; Jiang, H.; Zheng, J. A Novel Multi-Stage Stacked Triggering Method to Induce Progressive Failure Behaviors of Composite Corrugated Plate. *Appl. Compos. Mater.* **2020**, *27*, 55–74. [CrossRef]
3. Duan, L.; Xiao, N.-C.; Li, G.; Xu, F.; Chen, T.; Cheng, A. Bending analysis and design optimisation of tailor-rolled blank thin-walled structures with top-hat sections. *Int. J. Crashworthiness* **2017**, *22*, 227–242. [CrossRef]
4. Liu, Q.; Lin, Y.; Zong, Z.; Sun, G.; Li, Q. Lightweight design of carbon twill weave fabric composite body structure for electric vehicle. *Compos. Struct.* **2013**, *97*, 231–238. [CrossRef]
5. Abu Talib, A.R.; Ali, A.; Badie, M.A.; Azida Che Lah, N.; Golestaneh, A.F. Developing a hybrid, carbon/glass fiber-reinforced, epoxy composite automotive drive shaft. *Mater. Des.* **2010**, *31*, 514–521. [CrossRef]
6. Liu, Q.; Lu, Y.; Jiang, J.; Yan, X.; Li, Q. Experimental and numerical investigation into the dynamic impact responses of CFRP header rail. *Thin-Walled Struct.* **2022**, *181*, 110069. [CrossRef]
7. Babu, J.; Sunny, T.; Paul, N.A.; Mohan, K.P.; Philip, J.; Davim, J.P. Assessment of delamination in composite materials: A review. *Proc. Inst. Mech. Eng. Part B J. Eng. Manuf.* **2015**, *230*, 1990–2003. [CrossRef]
8. Davim, J.P.; Rubio, J.C.; Abrao, A.M. A novel approach based on digital image analysis to evaluate the delamination factor after drilling composite laminates. *Compos. Sci. Technol.* **2007**, *67*, 1939–1945. [CrossRef]
9. Lee, J.-M.; Lee, K.-H.; Kim, B.-M.; Ko, D.-C. Design of roof panel with required bending stiffness using CFRP laminates. *Int. J. Precis. Eng. Manuf.* **2016**, *17*, 479–485. [CrossRef]
10. Bambach, M.R. Fibre composite strengthening of thin steel passenger vehicle roof structures. *Thin-Walled Struct.* **2014**, *74*, 1–11. [CrossRef]
11. Borazjani, S.; Belingardi, G. Development of an innovative design of a composite-sandwich based vehicle roof structure. *Compos. Struct.* **2017**, *168*, 522–534. [CrossRef]
12. Borazjani, S.; Belingardi, G. Lightweight design: Detailed comparison of roof panel solutions at crash and stiffness analyses. *Int. J. Crashworthiness* **2017**, *22*, 49–62. [CrossRef]
13. Cheon, S.S.; Lee, D.G.; Jeong, K.S. Composite side-door impact beams for passenger cars. *Compos. Struct.* **1997**, *38*, 229–239. [CrossRef]
14. Wu, C.; Gao, Y.; Fang, J.; Lund, E.; Li, Q. Discrete topology optimization of ply orientation for a carbon fiber reinforced plastic (CFRP) laminate vehicle door. *Mater. Des.* **2017**, *128*, 9–19. [CrossRef]
15. Fang, X.; Li, D. Lightweight Concept Design of an Economical Multi-Material Vehicle Door with Fiber-Reinforced Thermoplastics. *Int. J. Automot. Technol.* **2023**, *24*, 719–737. [CrossRef]
16. Hasan, K.M.F.; Horváth, P.G.; Alpár, T. Potential fabric-reinforced composites: A comprehensive review. *J. Mater. Sci.* **2021**, *56*, 14381–14415. [CrossRef]
17. David Müzel, S.; Bonhin, E.P.; Guimarães, N.M.; Guidi, E.S. Application of the Finite Element Method in the Analysis of Composite Materials: A Review. *Polymers* **2020**, *12*, 818. [CrossRef]
18. Cheng, F.; Zheng, C.; Liu, Y.; Zuo, W.; Wang, X.; Guo, G. Lightweight Design of CFRP-Laminated Structures by Combining Microscopical Homogenization and Macroscopical Optimization. *Int. J. Automot. Technol.* **2021**, *22*, 1427–1436. [CrossRef]
19. Fang, G.; Qu, P.; Cao, Z.; Shi, F. Mechanical Analysis of Woven Composites Through Experimental Investigation and Multiscale Numerical Simulation. *Fibers Polym.* **2022**, *23*, 1440–1453. [CrossRef]
20. Gao, J.; Mojumder, S.; Zhang, W.; Li, H.; Suarez, D.; He, C.; Cao, J.; Liu, W.K. Concurrent n-scale modeling for non-orthogonal woven composite. *Comput. Mech.* **2022**, *70*, 853–866. [CrossRef]
21. Tang, S.F.; Huang, F.H.; Liang, J.; Du, S.Y. Multi-Scale Analysis for Thermo-Elasticity Properties of Composite Materials with Small Periodic Configuration. *Key Eng. Mater.* **2007**, *334–335*, 25–28. [CrossRef]
22. Yuan, Z.; Fish, J. Toward realization of computational homogenization in practice. *Int. J. Numer. Methods Eng.* **2008**, *73*, 361–380. [CrossRef]
23. Hong, J. Integrated Design of Structure and Material of Carbon Fiber Reinforced Plastics (CFRP). Master's Thesis, Hunan University, Changsha, China, 2018.
24. Ishikawa, T.; Chou, T.W. Stiffness and strength behaviour of woven fabric composites. *J. Mater. Sci.* **1982**, *17*, 3211–3220. [CrossRef]
25. Pochiraju, K.; Chou, T.-W. Three-dimensionally woven and braided composites. I: A model for anisotropic stiffness prediction. *Polym. Compos.* **1999**, *20*, 565–580. [CrossRef]
26. Whitney, T.J.; Chou, T.-W. Modeling of 3-D Angle-Interlock Textile Structural Composites. *J. Compos. Mater.* **1989**, *23*, 890–911. [CrossRef]
27. Li, G.; Xu, F.; Huang, X.; Sun, G. Topology Optimization of an Automotive Tailor-Welded Blank Door. *J. Mech. Des.* **2015**, *137*, 055001. [CrossRef]
28. Tsai, S.W.; Wu, E.M. A General Theory of Strength for Anisotropic Materials. *J. Compos. Mater.* **1971**, *5*, 58–80. [CrossRef]
29. Coello, C.A.C.; Lechuga, M.S. MOPSO: A proposal for multiple objective particle swarm optimization. In Proceedings of the 2002 Congress on Evolutionary Computation. CEC'02 (Cat. No.02TH8600), Honolulu, HI, USA, 12–17 May 2002. [CrossRef]
30. Ye, B.; Yu, G.; Zhang, Y.; Li, G. Structural Design of Aerostatic Bearing Based on Multi-Objective Particle Swarm Optimization Algorithm. *Appl. Sci.* **2023**, *13*, 3355. [CrossRef]
31. Davim, J.P. *Computational Methods and Production Engineering: Research and Development*; Woodhead Publishing: Shaxton, UK, 2017.
32. Davim, J.P. *Statistical and Computational Techniques in Manufacturing*; Springer Science & Business Media: Berlin/Heidelberg, Germany, 2012.

33. Goodarzi, E.; Ziaei, M.; Hosseinipour, E.Z. *Introduction to Optimization Analysis in Hydrosystem Engineering*; Springer: Berlin/Heidelberg, Germany, 2014.
34. Sun, G.; Zhang, H.; Fang, J.; Li, G.; Li, Q. Multi-objective and multi-case reliability-based design optimization for tailor rolled blank (TRB) structures. *Struct. Multidiscip. Optim.* **2017**, *55*, 1899–1916. [CrossRef]